Direct interactions between the secreted effector and the T2SS components GspL and GspM reveal a new effector-sensing step during type 2 secretion

Sandra Michel-Souzy, Badreddine Douzi, Frederic Cadoret, Claire Raynaud,
Loïc Quinton, Genevieve Ball, Romé Voulhoux

Direct interactions between the secreted effector and the T2SS components GspL and GspM reveal a new effector-sensing step during type 2 secretion

Sandra Michel-Souzy[#1], Badreddine Douzi[#1,2], Frédéric Cadoret[1], Claire Raynaud[1,2], Loïc Quinton[3], Geneviève Ball[1,2], and Romé Voulhoux*[1,2]

[1]: CNRS, Aix Marseille Université, IMM, LISM/UMR7255, Marseille, France

[2]: CNRS, Aix Marseille Université, IMM, LCB/UMR7283, Marseille, France

[3]: Laboratory of Mass Spectrometry - MolSys, Department of Chemistry, University of Liège, Liège, Belgium

[#] Contributed equally to this work.

Running title: Effector recognition in Type 2 secretion

* **Correspondence**: voulhoux@imm.cnrs.fr

ABSTRACT

In many Gram-negative bacteria, the type 2 secretion system (T2SS) plays an important role in virulence because of its capacity to deliver a large amount of fully folded protein effectors to the extracellular milieu. Despite our knowledge of most T2SS components, the mechanisms underlying effector recruitment and secretion by the T2SS remain enigmatic. Using complementary biophysical and biochemical approaches, we identified here two direct interactions between the secreted effector CbpD and two components, $XcpY_L$ and $XcpZ_M$, of the T2SS assembly platform (AP) in the opportunistic pathogen *Pseudomonas aeruginosa*. Competition experiments indicated that CbpD binding to $XcpY_L$ is $XcpZ_M$-dependent, suggesting sequential recruitment of the effector by the periplasmic domains of these AP components. Using the bacterial two-hybrid system, we then tested the influence of the effector on the AP protein-protein interaction network. Our findings revealed that the presence of the effector modifies the AP interactome and, in particular, induces $XcpZ_M$ homodimerization and increases the affinity between $XcpY_L$ and $XcpZ_M$. The observed direct relationship between effector binding and T2SS dynamics suggests an additional synchronizing step during the type 2 secretion process, where the activation of the AP of the T2SS nanomachine is triggered by effector binding.

INTRODUCTION

Type IV filament (Tff) nanomachines are membrane-embedded macromolecular complexes organized around a characteristic helical pilus-like structure emerging from an assembly platform at the cytoplasmic membrane (1). Tff are widespread in prokaryotes where they fulfill diverse cellular functions, in particular the type 2 secretion system (T2SS) that is found in many pathogenic Gram negative Proteobacteria (2). It is dedicated to the secretion of large folded periplasmic exoproteins via a piston-like apparatus called secreton. Secretons are constituted of 12 to 15 different components organized into 3 sub-complexes: the outer-membrane pore belonging to the secretin family, the assembly platform (AP) or motor of the

system, and the typical pseudopilus emerging from the AP up to the secretin pore (for the most recent reviews see (3,4)).

T2SS secretins are homomultimers assembled into a giant gated beta-barrel pore in the outer membrane (OM) connected to the AP by an N-terminal periplasmic extension (5-7). The Tff-specific structure of the T2SS is called pseudopilus. It is constituted by the helical assembly of the five pseudopilins of the system. Chronologically, the four minor pseudopilins GspHIJK are first assembled by the AP and thus form the head of the structure. This step is followed by the addition, from the bottom of the filament, of the major pseudopilin GspG into a pseudopilus (8-11). Pseudopilus assembly is energized and promoted by the AP, which is constituted by the oligomeric assembly of four membrane proteins including the three bitopic proteins GspC, GspL and GspM, and the integral membrane protein GspF. The energy for pseudopilus assembly is provided by the cytoplasmic ATPase, GspE. The four membrane components of the AP are interacting through a complex dynamic network involving both soluble and trans-membrane (TM) domains (12-17). GspC possesses an N-terminal TM domain anchoring the protein into the inner membrane (IM). GspC's TM domain is followed by a large C-terminal periplasmic domain composed of the HR and coiled-coil (or PDZ) sub-domains. GspC self-dimerizes through its TM sub-domain (13) and interacts with the N-domain of the secretin via its HR sub-domain (18,19), thus connecting the outer and inner membrane components of the secreton. The GspL and GspM AP components have a similar architecture with a TM domain followed by a globular C-terminal periplasmic domain with a ferredoxin-like fold (FLD) (15,16). These periplasmic domains self-interact but also interact with each other, as well as with the periplasmic domain of GspC (14,17). In contrast to GspM and GspC, GspL harbors an additional N-terminal cytoplasmic domain presenting structural homology with actin-like ATPases (20). This domain is, together with the integral inner membrane protein GspF, involved in the recruitment of the ATPase GspE at the secretion site (21-26). Further activation of GspE requires interactions with phospholipids (27). It has been proposed that upon sensing of a signal,

the AP interaction network is displaced to ensure proper functioning of the system possibly through intrinsic disorder domains (4). This includes signal transduction across the IM between the periplasmic and the cytoplasmic sides of the secreton (4,28). Such trans-membrane dynamic signaling has also been reported in the archetypal Tff member, the Type IV pilus (T4P) (29).

Type 2 secretion is a two steps process during which effectors are first exported across the IM by the Sec or Tat systems (30,31). Then, the folded periplasmic effectors are recognized and transported to the extracellular milieu by the secreton (32). How T2SS effectors are specifically recognized by secreton in the periplasmic soup remains an open question. In contrast to other secretion systems and in spite of intense research, no common secretion signal has indeed been identified in T2SS effectors. However, several direct interactions have been described between secreted effectors and the secretin GspD, the AP component GspC and the pseudopilus tip (24,33-36). It is accepted that effector recognition and recruitment is performed by GspC (17,24,34,37), followed by its transfer into the secretin vestibule before being extruded out of the cell upon contact with the pseudopilus tip (32). A direct interaction between effectors and GspC HR and PDZ sub-domains (24,37) suggests that effector recruitment involves multiple contacts with GspC. In addition, it has been shown that the TMHR domain of GspC is indirectly involved in effector recognition specificity in *P. aeruginosa* (17). Various GspD N-domains have also been involved in effector binding, depending on the organism (5,24,33,34,36). Finally, a direct interaction has also been reported between the effector and the pseudopilus tip constituted by the periplasmic domains of GspHIJK (34).

Here we report that in addition to interacting with GspC, the secretin and the pseudopilus tip, the T2SS secreted-effector also interacts specifically with the periplasmic domains of GspM and GspL inner membrane components of the AP. We further show that these periplasmic interactions trigger conformational changes into the AP that may lead to ATPase activation and pseudopilus assembly. We thus propose that these newly

2

discovered interactions constitute an additional step of the T2SS secretion process, synchronizing effector loading and pseudopilus assembly.

RESULTS

Direct and specific interaction between the Xcp effector CbpD and XcpY$_L$ periplasmic domain (XcpY$_L$p). Our T2SS working model is the Xcp system of *P. aeruginosa* where 11 different components are named P to Z with the species-specific prefix Xcp. Since protein letters are specific to the *Pseudomonas* genus, we will systematically refer to the general Gsp nomenclature using a subscript, *i.e.* the GspL homolog in *P. aeruginosa* is named XcpY$_L$.

We previously showed by Surface Plasmon Resonance (SPR) that the purified periplasmic domains of the secretin XcpQ$_D$, the AP component XcpP$_C$ and the pseudopilus tip quaternary complex (XcpU$_H$V$_I$W$_J$X$_K$) directly bind secreted effectors, thus allowing us to propose an integrated model of effector recognition and transport by the T2SS (34). In order to have a better view of the Xcp/effector interactome in the periplasm, we tested the interaction between the secreted effector CbpD and the periplasmic domains of the bitopic AP component XcpY$_L$ (XcpY$_L$p). We used BioLayer interferometry (BLI), an *in vitro* protein-protein interaction technique similar to SPR. XcpY$_L$p and CbpD proteins were produced and purified by consecutive affinity and size exclusion chromatography steps (Figure 1A), following the procedure previously used (34). CbpD was then biotinylated and immobilized on the sensor tip to be used as bait and interaction experiments were performed in triplicate with purified XcpY$_L$p used as prey following the protocol described in the experiment procedure section. The graph presented figure 1A and reporting the response (nm) as a function of the XcpY$_L$p concentration (μM) was used to measure the dissociation constants (K$_D$). BLI data reveal that XcpY$_L$p directly interacts with the secreted effector CbpD with a relatively low dissociation constant (K$_D$) of 5.0 μM.

To validate this *in vitro* interaction between CbpD and XcpY$_L$ in a more biological context, we set-up and performed an *in vivo* co-

purification experiment. In order to reconstitute the natural periplasmic context of the interaction in absence of the other Xcp T2SS components and secreted effectors, the two partners were produced in the periplasm of the heterologous host *Escherichia coli*. When produced in *E. coli*, CbpD naturally accumulates in the periplasm owing to its Sec signal peptide (Sp). The second partner XcpY$_L$p was artificially targeted to the periplasm by the addition of LasB Sp to its N-terminus (Sp-XcpY$_L$p). We first tested protein production under inducing conditions and verified the proper periplasmic localization of CbpD and XcpY$_L$p (Figure S1). The soluble cell fraction of the *E. coli*/pCbpD$_{H10}$/pSp-XcpY$_L$p strain grown under inducing conditions was extracted and analyzed by to Immobilized Metal Affinity Chromatography (IMAC). The co-purification experiments shown in figure 1B indicate that XcpY$_L$p is co-eluted with the histidine-tagged CbpD$_H$, used here as bait thus supporting the direct interaction found by BLi between the two proteins. The observation (Figure 1B bottom) that XcpY$_L$p is not recovered in the elution fractions in absence of CbpD$_H$, exclude a nonspecific affinity of XcpY$_L$p for the IMAC resin.

We then took advantage of the presence of two independent T2SS in *P. aeruginosa*, the Xcp and the Hxc systems, each secreting their own effectors (38), to test the effector specificity of this newly characterized interaction. We performed *in vivo* cross co-purification experiments using *E. coli* strains co-producing the Hxc effector LapA$_H$ together with XcpY$_L$p (*E. coli*/pLapA$_H$/pSp-XcpY$_L$p). Soluble proteins lysates obtained under inducible conditions were analysis by IMAC (Figure 1C) and we noticed that XcpY$_L$p did not co-purify with the heterologous Hxc effector. This data confirms that, as it is also the case for XcpQ$_D$, XcpP$_C$ and the pseudopilus tip (34), the interaction of XcpY$_L$ with its cognate effector is system specific.

Direct interaction between the Xcp effector CbpD and the periplasmic domain of XcpZ$_M$. In order to further characterize the Xcp/effector periplasmic interactome, we next tested if CbpD interacts with the periplasmic domain of the inner membrane component

3

$XcpZ_M$ ($XcpZ_Mp$). $XcpZ_M$ corresponds to the only periplasmic globular domain of the secreton not yet tested for interaction with the secreted effector. As above for $XcpY_L$, we combined complementary *in vitro* and *in vivo* protein-protein interaction experiments to investigate the interaction between $XcpZ_Mp$ and secreted effectors. The BLI experiment using purified CbpD as bait and $XcpZ_Mp$ as prey was done in triplicate and showed a direct interaction between the two proteins, with a dissociation constant (K_D) of 3.4 μM (Figure 2A). This *in vitro* interaction was confirmed by cross-linking experiment using the short cross-linking agent BS2G. Analysis of the cross-linking products by SDS-PAGE followed by Coomassie blue staining showed a protein complex specifically recovered in presence of the two partners and the cross-linker (Figure S2), with a molecular weight corresponding to a heterodimer composed of $XcpZ_Mp$ and CbpD. This was confirmed by immunoblotting, which showed that $XcpZ_Mp$ and CbpD are both present in the corresponding complex.

Furthermore, the interaction between $XcpZ_Mp$ and CbpD was tested and validated by *in vivo* co-purification experiments. To do this, we constructed an *E. coli* strain producing in its periplasm $CbpD_H$ and $XcpZ_Mp$ (*E. coli*/$pCbpD_H$/$pSp-XcpZ_Mp$), and proceeded with IMAC co-purification experiments following the procedure used for $XcpY_Lp$.
The analysis of the eluted fractions by SDS-PAGE followed by immunoblotting with anti-CbpD and anti-$XcpZ_M$ antibodies shows the specific co-elution of $XcpY_Lp$ by $CbpD_H$ (Figure 2B). As for $XcpY_Lp$ the $XcpZ_Mp$/effector interaction is Xcp T2SS specific since the Hxc effector $LapA_H$ does not co-purify the Xcp GspM component $XcpZ_Mp$ (Figure 2C).

Altogether, the presently discovered direct interactions between the secreted effector and the globular periplasmic domains of $XcpZ_M$ and $XcpY_L$ reveal for the first time a direct and specific interaction between secreted effector and components of the T2SS assembly platform.

Competition between $XcpY_Lp$ and $XcpZ_Mp$ for binding to CbpD. Protein-protein interaction data revealed that the AP components $XcpY_L$ and $XcpZ_M$ interact directly with the effector through their periplasmic domains, which raises to five the number of Xcp periplasmic domains or complexes that directly and specifically interact with secreted effectors. In all cases, interaction affinities between T2SS components and the secreted effector are in the μM range, in agreement with their transiency during the secretion process. We attempted to better understand the $CbpD$/$XcpY_Lp$/$XcpZ_Mp$ interactome by evaluating possible competition effects thanks to the multiple co-expression capacity of our *in vivo* periplasmic reconstitution effector/Xcp interactome assay. We therefore quantitatively compared the co-purification levels of $XcpY_Lp$ and $XcpZ_Mp$ with $CbpD_H$ in presence or not of the other CbpD interactant. Hence the soluble cell lysates of the *E. coli* strains co-producing $CbpD_H$ with $XcpY_Lp$, $XcpZ_Mp$ or $XcpY_Lp$ together with $XcpZ_Mp$ were generated in quadruplicates and analyzed by IMAC for $XcpZ_Mp$ and $XcpY_Lp$ co-purification (Figure 3). While the proportion of $XcpZ_Mp$ co-purified with CbpD is unchanged with or without co-production of $XcpY_Lp$ (Figure 3 grey bars and corresponding immunoblots), a statistically significant reduction of $XcpY_Lp$ binding to CbpD was observed in the presence of $XcpZ_Mp$ (Figure 3 black bars and corresponding immunoblots). This competition experiment suggests that, during the secretion process, the secreted effector interact sequentially with $XcpY_L$ and $XcpZ_M$.

CbpD effector triggers $XcpZ_M$ dimerization and increases $XcpZ_M$-Y_L interaction. The above data indicate that both $XcpY_L$ and $XcpZ_M$ interact with the secreted effector through their periplasmic domains. In order to understand the possible consequences of such interactions on the global AP interactome within the secreton, we used the bacterial adenylate cyclase two-hybrid (BACTH) method developed by Karimova and collaborators (39). In this technique, proteins of interest are co-expressed in an *E. coli cya* mutant (BTH101) as fusions with one of the two fragments (T18 and T25) from the catalytic domain of *Bordetella pertussis* adenylate cyclase. Interaction of two-hybrid proteins results in a functional complementation between T18 and T25 leading to cAMP synthesis, and transcriptional activation

4

of the lactose operon that can be easily detected by β-galactosidase activity measurement. We have chosen this technique since it is particularly well adapted to quantify interactions between membrane proteins (40). Full-length $XcpY_L$, Z_M and S_F proteins were therefore fused to the T18 and/or T25 domains via their N-termini (see experimental procedure).

We firstly evaluated the hetero-dimerization capacities of different AP components by measuring β-galactosidase activity of the three $T18-Y_L/T25-S_F$, $T18-Y_L/T25-Z_M$ and $T18-Z_M/T25-S_F$ combinations, and comparing it to positive and negative controls (Figure 4 light grey bars). This indicates that full-length $XcpY_L$ directly interacts with $XcpZ_M$. A similar observation, using the same approach, was already reported in different T2SSs (10, 11, 14). Interestingly, we also found that $XcpS_F$, the polytopic IM component of the AP directly interacts with $XcpY_L$ and $XcpZ_M$, thus confirming the physical interconnection between components of the AP. In addition and as previously observed by Lallemand and collaborators (14), full-length $XcpZ_M$ does not, or very weakly, self-dimerize when produced alone in the *E. coli* membrane (Figure 4). This negative result is not due to non-functional fusion proteins since both T18/25 $XcpZ_M$ fusions give positive signals when combined with $XcpY_L$ and $XcpS_F$ partners (Figure 4). This result contrasts with the homo-dimerization property of the periplasmic domain of $XcpZ_M$ revealed by size exclusion chromatography (Figure S3), and suggests that $XcpZ_M$ periplasmic homo-dimerization might be prevented by its transmembrane domain.

We then decided to challenge this AP interactome in presence of the T2SS effector CbpD (Figure 4 dark grey bars). CbpD was therefore co-produced in the periplasm of the BTH101 strains producing the various Xcp T18/T25 pairs. No difference was seen for the pairs involving $XcpS_F$, indicating that CbpD binding to $XcpY_L$ has no significant effect on the $XcpY_L/S_F$ interaction. On the other hand, a statistically significant increase in β-galactosidase activity was measured in presence of CbpD for the $T18-Z_M/T25-Z_M$ pair, showing that the presence of CbpD triggers $XcpZ_M$ homo-dimerization, possibly through their periplasmic

domains (Figure S3). Similarly, CbpD co-production was also performed with the $T18-Y_L/T25-Z_M$ pair. In this case, the presence of the effector significantly increases the β-galactosidase levels, revealing a significant strengthening of the interaction between $XcpY_L$ and $XcpZ_M$ in presence of the secreted effector. Those findings indicate that the presence of the effector triggers structural re-arrangements of the AP, thus suggesting a possible synchronization between effector arrival and activation of the system.

DISCUSSION

Effector recognition by the T2SS remains enigmatic since no common secretion signal has been identified in the numerous effectors reported so far. All attempts to identify the secretion signal of the T2SS have converged to the existence of a still unknown conformational signal, in agreement with the folded state of the effectors prior recognition by the secreton (41). Here, we focused on the Xcp T2SS of *P. aeruginosa,* which secretes at least 19 different exoproteins, to study effector recognition and transport. Based on the identification of a set of direct periplasmic interactions between secreted effectors and components of the three sub-complexes of the secreton, we previously proposed a model of effector recognition and transport by the T2SS (34). In this model, the substrate is recognized by the secreton peripheral component $XcpP_C$ and then transferred into the secretin ($XcpQ_D$) vestibule in order to be expelled out of the secretin pore upon contact with the pseudopilus tip ($XcpU_HV_IW_JX_K$). In the present study, we completed the Xcp/effector periplasmic interactome by testing $XcpY_L$ and $XcpZ_M$, the last two Xcp components harboring a periplasmic domain not included in previous studies. We applied two complementary protein-protein interaction approaches and found that the two AP components directly and specifically interact with the secreted effector CbpD through their periplasmic domains. This brings to five the number of Xcp partners physically and specifically encountered by the effector during the secretion process, thus indicating a system-

specific route for substrate recruitment and transport all along the Xcp T2SS secreton.

IMAC experiments revealed a competition between $XcpY_L$ and $XcpZ_M$ for the effector, suggesting interaction sequentiality. It is however difficult at this stage to establish an order for these two interactions and propose a hierarchical positioning in the previous T2SS secretion model. Our data nevertheless show for the first time a direct involvement of both GspL and GspM in substrate recognition.

We further evaluated the possible consequences of these new interactions on the T2SS by addressing their impact on AP dynamics. Using BACTH as a quantitative protein-protein interaction technic, we first established the interactome network between the three AP components $XcpY_L$, $XcpZ_M$ and $XcpS_F$. We then found that $XcpZ_M$ oligomerization and $XcpY_L$/$XcpZ_M$ hetero-dimerization are respectively triggered and strengthened upon effector binding. Those important observations constitute the first experimental evidence of effector-mediated conformational changes of the T2SS AP components, suggesting a possible synchronization between effector arrival and activation of the system. One possible type of activation mediated by substrate binding was described in a recent paper by Lallemand and collaborators (14). In this work, using an elegant combination of *in vivo* protein-protein interaction and cross-linking experiments, the authors showed the molecular details of the dynamic interplay between full-length GspL and GspM. In their model, upon sensing an unknown signal, the interactions between GspL and GspM periplasmic domains are shifting from homo- to hetero-dimers, mediating coordinated shifts or rotations of their cognate TM domains. We propose that the dynamic interplay leading to signal transduction from the periplasm to the cytoplasm is triggered by effector binding on GspM and/or GspL periplasmic domain. It would be interesting to localize the effector-binding domains in $XcpY_L$ and $XcpZ_M$ and their possible overlapping with the ferredoxin-like domains (FLD) of GspL and GspM, directly involved in the dynamic interplay.

The next obvious question brought by our observations is what is the target of the signal transduced from the periplasm to the cytoplasm? A possible scenario, elaborated from the numerous interactions reported between the cytoplasmic domain of GspL and its partner, the ATPase GspE, was recently proposed by Gu and collaborator (4). Taking into account that activation of the ATPase necessitates an interaction between membrane lipids and the GspL's segment adjacent to the TM domain (27), the authors propose that activation of the ATPase could be mediated by a displacement of GspL in the inner membrane, itself induced by the transmembrane signal generated by effector binding in the periplasm. Therefore, considering that activation of the ATPase mediates pseudopilus assembly (42, 43), we propose that effector binding on the periplasmic domains of GspL and GspM triggers pseudopilus assembly, thus synchronizing this late step with effector arrival in the machinery. Therefore, an additional effector-sensing step, coupled with pseudopilus assembly, can be added to our model of effector recognition and transport by the T2SS (Figure 5). Whether this effector sensing-step mediated by GspL and GspM is linked with their direct involvement in pseudopilus assembly (10,43) remains to be determined.

Further investigations are now required to understand at molecular level, the chronology of the interactions effector/$XcpY_L$ and effector/$XcpZ_M$ and the effector subsequent transition into the vestibule of the secretin, as well as the structural basis of the trans-membrane signal transduction. In this respect, interestingly, the $XcpY_L$ periplasmic domain presents structural homology with proteins harboring the Per-Arnt-Sim (PAS) domain. These PAS domains are present in all three domains of life and are involved in signaling and transmembrane signal transduction, such as in the bacterial two-component systems (44). This structural homology supports the sensing properties of GspL which may play an important role in T2SS function.

EXPERIMENTAL PROCEDURES

Bacterial strains & Plasmids. Bacterial strains and plasmids used in this study are listed in Table 1.

DNA manipulation. Plasmid preparation, DNA purification, gel extraction

and PCR product purification were performed using appropriate Macherey Nagel kits. Restriction enzymes, DNA polymerase and other molecular biology reagents were purchased from New England Biolabs or Promega. The high fidelity polymerase Q5 (Biolabs) was used for PCR amplification. The list of oligonucleotides (synthesized by IDT) used for cloning is provided in Table 2. To construct the BACTH plasmids, the *xcp* genes were PCR-amplified using corresponding primers, and cloned into pKT25 and pUT18C vectors using SLIC method between BamHI and EcoRI sites. To construct the expression plasmids for heterologous reconstitution, the $xcpY_L$ and $xcpZ_M$ genes were PCR-amplified using corresponding primers, and cloned into the pCDFDuet vector using SLIC method or digestion ligation methods between NcoI-SalI (MCS1) sites for $XcpZ_Mp$ or NdeI-EcoRV (MCS2) sites for $XcpY_Lp$. The gene of $CbpD_H$ was subcloned from pT7.5 vector to pETDuet vector thanks EcoRI site. All plasmids were sequenced by GATC Company.

Protein production and purification. The DNA sequences encoding for the periplasmic domains of $XcpY_L$ ($XcpY_Lp$: from residue 255 to residue 381) and $XcpZ_M$ ($XcpZ_Mp$: from residue 53 to residue 173) were cloned into pLIC07 vector using SLIC method between BsaI sites. These constructs allow the production of $XcpY_Lp$ and $XcpZ_Mp$ proteins fused to the Thioredoxin (Trx) at their N-terminus. The Trx is cleaved off after purification and the resulting proteins are soluble, stable and produced in sufficient amount for biochemical and biophysical characterization. Competent cells of strain BL21 (DE3) were transformed with pLIC-$XcpZ_Mp$ or pLIC-$XcpY_Lp$. The bacteria were grown until 0.5 OD_U (Optical Density Units at 600 nm) at 37°C on TB medium with Kanamycin (Km) at 50 µg/ml. The induction was performed with 0.1 mM of IPTG during 12h at 25°C. Bacteria were collected by centrifugation and broken by sonication (4 x 1min) in cold buffer Tris-HCl pH 8 50 mM, NaCl 300 mM, EDTA 1 mM, $MgCl_2$ 20 mM, PMSF 1 mM, lysozyme 0.5 mg/ml, DNAse 20 µg/ml, imidazole 10 mM. The lysate was cleared by ultracentrifugation (20,000 x g) to remove unbroken debris and membranes. The cleared lysate containing Trx-$XcpY_Lp$ and Trx-$XcpZ_Mp$ were loaded onto a 5-ml Nickel column (HisTrap™ FF) using an ÄKTA prime apparatus (GE healthcare) and the immobilized proteins were eluted in buffer B (50 mM Tris-HCl pH 8.0, 300 mM NaCl, 500 mM imidazole). $XcpY_Lp$ and $XcpZ_Mp$ were obtained after cleavage of the Trx fusion using 2 mg of TEV protease for 18 hours at 4°C and dialysis in a dialysis bag to remove imidazole. Untagged soluble proteins were then collected in the flow-through of a 5-ml Nickel column while the histidine-tagged Tev and Trx proteins remain bound to the column. The proteins were concentrated using the centricon technology (Millipore, 10-kDa cut-off) and subjected to size exclusion chromatography (SEC) purification using a HiLoad Superdex200 16/600 column pre-equilibrated with 50 mM Tris-HCl pH 8, 150 mM NaCl.

For CbpD, the extraction and the purification protocols of the periplasmic material were described previously (5).

Purity and quality of the purified proteins were checked by analyzing samples by SDS-PAGE followed by Coomassie blue staining.

SDS-PAGE and immuno-detection. Proteins from bacterial extracts were separated by electrophoresis on 15% or 18% of polyacrylamide gels and transferred onto nitrocellulose membranes using a semi-dry blotting apparatus. Membranes were blocked with 5% milk in TBST (10 mM Tris, 150 mM NaCl, 0.05% Tween 20) or in PBS. Membranes were incubated with rabbit polyclonal antibody directed against CbpD, $XcpY_L$, $XcpZ_M$ and LapA (respectively diluted at 1:5000, 1:1500, 1:500 and 1:5000 in TBST-5% milk). The incubation was followed by two 10-min washes and incubation in peroxidase-coupled anti-rabbit antibody (1:5000, Sigma). Membranes were developed by homemade enhanced chemiluminescence and scanned using ImageQuant TL analysis software (GE Healthcare Life sciences).

Co-production of $XcpY_p$, $XcpZ_p$, $LapA_H$ and $CbpD_H$ in E. coli and affinity chromatography. Competent cells of strain BL21 (DE3) were co-transformed with pCDFDuet, pETDuet and derivatives. The

bacteria were grown until 0,5 OD at 600 nm at 37°C on LB or TB medium with antibiotics appropriate (Streptomycin 30 µg/ml, Ampicillin 50 µg/ml). The induction was performed with 0,1 mM of IPTG during 12h at 17°C or 25°C. Bacteria were collected by centrifugation and broken by French Press (10,000 psi) in cold buffer Tris-HCl pH 8 50 mM, NaCl 150 mM, EDTA 1 mM, $MgCl_2$ 20 mM, PMSF 1 mM, lysosyme 0.5 mg/ml, DNAse 20 µg/ml. The lysate was cleared by ultracentrifugation to remove unbroken debris and membranes. The cleared lysate was loaded onto a 1-ml Nickel column (HisTrap™ FF) using an ÄKTA prime apparatus (GE healthcare). The immobilized proteins were eluted in buffer B (50 mM Tris-HCl pH 8, 150 mM NaCl, 500 mM imidazole). The loaded (L), flow through (FT) and elution (E) fractions were analyzed by SDS-PAGE and immunodetection. For competition experiments, the complete CbpD co-purification IMAC procedure for $XcpY_L$, $XcpZ_M$ and $XcpY_L$ together with $XcpZ_M$ was performed in quadruplicate. The total amount of $XcpY_L$ or $XcpZ_M$ proteins in the eluate (E) fractions (in % from the total amount in the load (L) fraction) was measured and quantified from immunoblots of each replicate using ImageJ software. Microsoft Excel software was used for data processing and presentation. Statistics were determined using the Student's t-test function of Excel using a bilateral model and assuming equal variance.

Bio-layer Interferometry. CbpD was biotinylated using the EZ-Link NHS-PEG4-Biotin kit (Perbio Science, France) with a 1:1 molar ratio (CbpD:Biotin). The reaction was stopped by removing the excess of the biotin using a Zeba Spin Desalting column (Perbio Science, France). BLI studies were performed in triplicate in black 96-well plates (Greiner) at 25°C using an OctetRed96 (ForteBio, USA). Streptavidin biosensor tips (ForteBio, USA) were first hydrated with 0.2 ml of interaction buffer (IB) (1X Kinetics Buffer ForteBio diluter in PBS) for 20 min and then loaded with biotinylated protein (CbpD at 5 µg/ml in IB). To study the binding of CbpD to $XcpY_Lp$ or $XcpZ_Mp$, increasing concentrations of $XcpY_Lp$ (5 to 160 µM) and $XcpZ_Mp$ (6,25 to 100µM) were

used and the association and dissociation phases were monitored for 1000 sec and 3000 sec, respectively. Xcp proteins were dialyzed against IB before titration experiments. To avoid the non-specific binding of $XcpY_Lp$ or $XcpZ_Mp$ to the SA bio-sensors, the bio-sensors were incubated with 10ug/mL of Biocytin (Sigma) for 200 sec. In all experiments, the response of the non-biotinylated proteins on the free sensors was subtracted during experiment processing.

The dissociation constants (K_D) was calculated using the GraphPad Prism 5.0 software on the basis of the steady state levels of the responses on nm, directly related to the concentration of the Xcp protein. The K_D was calculated from a triplicate experiment by plotting on x axis the different concentration of the Xcp protein and the different responses of the Xcp protein at the saturation (990 sec after the start of the association step) on the y axis. For K_D calculation, nonlinear regression fit for xy analysis was used and one binding site (specific binding) as a model which corresponds to the equation $y = Bmax \times x/(K_D + x)$.

Bacterial two-hybrid and statistical analysis. To investigate the interaction between $XcpZ_M$ and $XcpY_L$ periplasmic domains, competent cells of strain BTH101 were co-transformed with pUT18C and pKT25 derivatives and bacteria were grown for 48 h at 30°C on LB plates containing Ap100, Kan50 and Sm100. Colonies were picked at random and inoculated into 600 µl cultures in LB containing Amp100, Kan50 and Sm100 and 0.5 mM IPTG and grown overnight at 30°C. ß-galactosidase activity was measured as described (45). At least 2 independent experiments were performed with 3 randomly picked transformants. Mean values were presented by bar graphs, and error bars indicate standard deviation. Microsoft Excel software was used for data processing and presentation. Statistics were determined using the Student's t-test function of excel using a bilateral model and assuming equal variance.

To study the interaction network between the full-length proteins, competent cells of BTH101 containing pJN105 or pJN105-CbpD vectors were co-transformed with pUT18C and pKT25 derivates. Bacteria were grown for 48 h at 30°C on LB plates containing Ap100, Km50,

8

Sm100 and Gm15. Colonies were picked at random and inoculated into 600 µl cultures in LB containing Ap100, Km50, Sm100, Gm15, 0.5mM IPTG and 0.5% Arabinose to allow CbpD production. Cells were grown overnight at 30°C and ß-galactosidase activity was measured as described (45).

CONFLICTS OF INTEREST

The authors declare no conflict of interest.

AUTHOR CONTRIBUTIONS

RV, SMS, BD conceived the project; RV, SMS, BD, FC, CR, GB, LQ performed experimental studies and RV, SMS, BD wrote the manuscript.

REFERENCES

1. Berry, J. L., and Pelicic, V. (2015) Exceptionally widespread nanomachines composed of type IV pilins: the prokaryotic Swiss Army knives. *FEMS microbiology reviews* **39**, 134-154

2. Cianciotto, N. P., and White, R. C. (2017) Expanding Role of Type II Secretion in Bacterial Pathogenesis and Beyond. *Infection and immunity* **85,** doi: 10.1128/IAI.00014-17

3. Thomassin, J. L., Santos Moreno, J., Guilvout, I., Tran Van Nhieu, G., and Francetic, O. (2017) The trans-envelope architecture and function of the type 2 secretion system: new insights raising new questions. *Molecular microbiology* **105**, 211-226

4. Gu, S., Shevchik, V. E., Shaw, R., Pickersgill, R. W., and Garnett, J. A. (2017) The role of intrinsic disorder and dynamics in the assembly and function of the type II secretion system. *Biochimica et biophysica acta* **1865**, 1255-1266

5. Douzi, B., Trinh, N. T. T., Michel-Souzy, S., Desmyter, A., Ball, G., Barbier, P., Kosta, A., Durand, E., Forest, K. T., Cambillau, C., Roussel, A., and Voulhoux, R. (2017) Unraveling the self-assembly of the *Pseudomonas aeruginosa* XcpQ secretin periplasmic domain provides new molecular insights into T2SS secreton architecture and dynamics. *mBio* **8,** doi: 10.1128/mBio.01185-17

6. Hay, I. D., Belousoff, M. J., and Lithgow, T. (2017) Structural basis of Type 2 Secretion System engagement between the inner and outer bacterial membranes. *mBio* **8**, e01344-01317

7. Yan, Z., Yin, M., Xu, D., Zhu, Y., and Li, X. (2017) Structural insights into the secretin translocation channel in the type II secretion system. *Nature structural & molecular biology* **24**, 177-183

9

8. Douzi, B., Durand, E., Bernard, C., Alphonse, S., Cambillau, C., Filloux, A., Tegoni, M., and Voulhoux, R. (2009) The XcpV/GspI pseudopilin has a central role in the assembly of a quaternary complex within the T2SS pseudopilus. *The Journal of biological chemistry* **284**, 34580-34589

9. Cisneros, D. A., Bond, P. J., Pugsley, A. P., Campos, M., and Francetic, O. (2012) Minor pseudopilin self-assembly primes type II secretion pseudopilus elongation. *The EMBO journal* **31**, 1041-1053

10. Nivaskumar, M., Santos-Moreno, J., Malosse, C., Nadeau, N., Chamot-Rooke, J., Tran Van Nhieu, G., and Francetic, O. (2016) Pseudopilin residue E5 is essential for recruitment by the type 2 secretion system assembly platform. Molecular microbiology 101, 924-941

11. Santos-Moreno, J., East, A., Guilvout, I., Nadeau, N., Bond, P. J., Tran Van Nhieu, G., and Francetic, O. (2017) Polar N-terminal Residues Conserved in Type 2 Secretion Pseudopilins Determine Subunit Targeting and Membrane Extraction Steps during Fibre Assembly. Journal of molecular biology 429, 1746-1765

12. Sandkvist, M., Hough, L. P., Bagdasarian, M. M., and Bagdasarian, M. (1999) Direct interaction of the EpsL and EpsM proteins of the general secretion apparatus in *Vibrio cholerae*. *Journal of bacteriology* **181**, 3129-3135

13. Login, F. H., and Shevchik, V. E. (2006) The single transmembrane segment drives self-assembly of OutC and the formation of a functional type II secretion system in *Erwinia chrysanthemi*. *The Journal of biological chemistry* **281**, 33152-33162

14. Lallemand, M., Login, F. H., Guschinskaya, N., Pineau, C., Effantin, G., Robert, X., and Shevchik, V. E. (2013) Dynamic interplay between the periplasmic and transmembrane domains of GspL and GspM in the type II secretion system. *PloS one* **8**, e79562

15. Abendroth, J., Rice, A. E., McLuskey, K., Bagdasarian, M., and Hol, W. G. (2004) The crystal structure of the periplasmic domain of the type II secretion system protein EpsM from *Vibrio cholerae*: the simplest version of the ferredoxin fold. *Journal of molecular biology* **338**, 585-596

16. Abendroth, J., Kreger, A. C., and Hol, W. G. (2009) The dimer formed by the periplasmic domain of EpsL from the Type 2 Secretion System of Vibrio parahaemolyticus. *Journal of structural biology* **168**, 313-322

17. Gerard-Vincent, M., Robert, V., Ball, G., Bleves, S., Michel, G. P., Lazdunski, A., and Filloux, A. (2002) Identification of XcpP domains that confer functionality and specificity to the *Pseudomonas aeruginosa* type II secretion apparatus. *Molecular microbiology* **44**, 1651-1665

18. Korotkov, K. V., Johnson, T. L., Jobling, M. G., Pruneda, J., Pardon, E., Heroux, A., Turley, S., Steyaert, J., Holmes, R. K., Sandkvist, M., and Hol, W. G. (2011) Structural and functional studies on the interaction of GspC and GspD in the type II secretion system. *PLoS pathogens* **7**, e1002228

19. Wang, X., Pineau, C., Gu, S., Guschinskaya, N., Pickersgill, R. W., and Shevchik, V. E. (2012) Cysteine scanning mutagenesis and disulfide mapping analysis of arrangement of GspC and GspD protomers within the type 2 secretion system. *The Journal of biological chemistry* **287**, 19082-19093

20.   Abendroth, J., Bagdasarian, M., Sandkvist, M., and Hol, W. G. (2004) The structure of the cytoplasmic domain of EpsL, an inner membrane component of the type II secretion system of *Vibrio cholerae*: an unusual member of the actin-like ATPase superfamily. *Journal of molecular biology* **344**, 619-633

21.   Abendroth, J., Mitchell, D. D., Korotkov, K. V., Johnson, T. L., Kreger, A., Sandkvist, M., and Hol, W. G. (2009) The three-dimensional structure of the cytoplasmic domains of EpsF from the type 2 secretion system of *Vibrio cholerae*. *Journal of structural biology* **166**, 303-315

22.   Ball, G., Chapon-Herve, V., Bleves, S., Michel, G., and Bally, M. (1999) Assembly of XcpR in the cytoplasmic membrane is required for extracellular protein secretion in *Pseudomonas aeruginosa*. *Journal of bacteriology* **181**, 382-388

23.   Chen, Y. L., and Hu, N. T. (2013) Function-related positioning of the type II secretion ATPase of *Xanthomonas campestris* pv. campestris. *PloS one* **8**, e59123

24.   Pineau, C., Guschinskaya, N., Robert, X., Gouet, P., Ballut, L., and Shevchik, V. E. (2014) Substrate recognition by the bacterial type II secretion system: more than a simple interaction. *Molecular microbiology* **94**, 126-140

25.   Lu, C., Korotkov, K. V., and Hol, W. G. (2014) Crystal structure of the full-length ATPase GspE from the Vibrio vulnificus type II secretion system in complex with the cytoplasmic domain of GspL. *Journal of structural biology* **187**, 223-235

26.   Shiue, S. J., Kao, K. M., Leu, W. M., Chen, L. Y., Chan, N. L., and Hu, N. T. (2006) XpsE oligomerization triggered by ATP binding, not hydrolysis, leads to its association with XpsL. *The EMBO journal* **25**, 1426-1435

27.   Camberg, J. L., Johnson, T. L., Patrick, M., Abendroth, J., Hol, W. G., and Sandkvist, M. (2007) Synergistic stimulation of EpsE ATP hydrolysis by EpsL and acidic phospholipids. *The EMBO journal* **26**, 19-27

28.   Campos, M., Cisneros, D. A., Nivaskumar, M., and Francetic, O. (2013) The type II secretion system - a dynamic fiber assembly nanomachine. *Research in microbiology* **164**, 545-555

29.   Leighton, T. L., Yong, D. H., Howell, P. L., and Burrows, L. L. (2016) Type IV Pilus Alignment Subcomplex Proteins PilN and PilO Form Homo- and Heterodimers in Vivo. *The Journal of biological chemistry* **291**, 19923-19938

30.   Pugsley, A. P., Kornacker, M. G., and Poquet, I. (1991) The general protein-export pathway is directly required for extracellular pullulanase secretion in *Escherichia coli* K12. *Molecular microbiology* **5**, 343-352

31.   Voulhoux, R., Ball, G., Ize, B., Vasil, M. L., Lazdunski, A., Wu, L. F., and Filloux, A. (2001) Involvement of the twin-arginine translocation system in protein secretion via the type II pathway. *The EMBO journal* **20**, 6735-6741

32.   Douzi, B., Filloux, A., and Voulhoux, R. (2012) On the path to uncover the bacterial type II secretion system. *Philosophical transactions of the Royal Society of London. Series B, Biological sciences* **367**, 1059-1072

33.   Shevchik, V. E., Robert-Baudouy, J., and Condemine, G. (1997) Specific interaction between OutD, an *Erwinia chrysanthemi* outer membrane protein of the general secretory pathway, and secreted proteins. *The EMBO journal* **16**, 3007-3016

34.   Douzi, B., Ball, G., Cambillau, C., Tegoni, M., and Voulhoux, R. (2011) Deciphering the Xcp *Pseudomonas aeruginosa* type II secretion machinery through multiple interactions with substrates. *The Journal of biological chemistry* **286**, 40792-40801

35.   Reichow, S. L., Korotkov, K. V., Gonen, M., Sun, J., Delarosa, J. R., Hol, W. G., and Gonen, T. (2011) The binding of cholera toxin to the periplasmic vestibule of the type II secretion channel. *Channels* **5**, 215-218

36.   Reichow, S. L., Korotkov, K. V., Hol, W. G., and Gonen, T. (2010) Structure of the cholera toxin secretion channel in its closed state. *Nature structural & molecular biology* **17**, 1226-1232

37.   Bouley, J., Condemine, G., and Shevchik, V. E. (2001) The PDZ domain of OutC and the N-terminal region of OutD determine the secretion specificity of the type II out pathway of *Erwinia chrysanthemi*. *Journal of molecular biology* **308**, 205-219

38.   Ball, G., Durand, E., Lazdunski, A., and Filloux, A. (2002) A novel type II secretion system in *Pseudomonas aeruginosa*. *Molecular microbiology* **43**, 475-485

39.   Karimova, G., Pidoux, J., Ullmann, A., and Ladant, D. (1998) A bacterial two-hybrid system based on a reconstituted signal transduction pathway. *Proceedings of the National Academy of Sciences of the United States of America* **95**, 5752-5756

40.   Georgiadou, M., Castagnini, M., Karimova, G., Ladant, D., and Pelicic, V. (2012) Large-scale study of the interactions between proteins involved in type IV pilus biology in *Neisseria meningitidis*: characterization of a subcomplex involved in pilus assembly. *Molecular microbiology* **84**, 857-873

41.   Sandkvist, M. (2001) Biology of type II secretion. *Molecular microbiology* **40**, 271-283

42.   Nivaskumar, M., Bouvier, G., Campos, M., Nadeau, N., Yu, X., Egelman, E. H., Nilges, M., and Francetic, O. (2014) Distinct docking and stabilization steps of the Pseudopilus conformational transition path suggest rotational assembly of type IV pilus-like fibers. *Structure* **22**, 685-696

43.   Gray, M. D., Bagdasarian, M., Hol, W. G., and Sandkvist, M. (2011) In vivo cross-linking of EpsG to EpsL suggests a role for EpsL as an ATPase-pseudopilin coupling protein in the Type II secretion system of *Vibrio cholerae*. Molecular microbiology 79, 786-798

44.   Henry, J. T., and Crosson, S. (2011) Ligand-binding PAS domains in a genomic, cellular, and structural context. *Annual review of microbiology* **65**, 261-286

45.   Miller, J.H. (1972) Experiments in Molecular Genetics, Cold Spring Harbor, NY: Cold Spring Harbor Laboratory.

46.   Douzi, B., Brunet, Y. R., Spinelli, S., Lensi, V., Legrand, P., Blangy, S., Kumar, A., Journet, L., Cascales, E., and Cambillau, C. (2016) Structure and specificity of the Type VI secretion system ClpV-TssC interaction in enteroaggregative *Escherichia coli*. *Scientific reports* **6**, 34405

47.   Cadoret, F., Ball, G., Douzi, B., Voulhoux, R. (2014). Txc, a new type II secretion system of *Pseudomonas aeruginosa* strain PA7, is regulated by the TtsS/TtsR two-component system and directs specific secretion of the CbpE chitin-binding protein. J Bacteriol **196**, 2376-2386.

48.   Newman JR, Fuqua C. 1999. Broad-host-range expression vectors that carry the L-arabinose inducible *Escherichia coli araBAD* promoter and the *araC* regulator. Gene **227,** 197-203.

Table 1 - Bacterial strain and plasmids used in this study

Strain & plasmids	Genotype/Characteristics	Origin
E. coli		
BL21 (DE3)	*fhuA2 [lon] ompT gal (λ DE3) [dcm]λ DE3 λ sBamHIo ΔEcoRI-B int::(lacI::PlacUV5::T7 gene1)*	Lab. collection
TG1	*supE, hsdΔR, thiΔ (lac⁻proAB), F' (traD36, proAB+, lacIq, lacZΔM15)*	Lab. collection
BTH101	*F⁻, cya-99, araD139, galE15, galK16, rpsL1 (Strʳ), hsdR2, mcrA1, mcrB1*	Lab. collection
P. aeruginosa		
PAO1	Clinical isolate, reference wild-type strain	Lab. collection
PAO1 D40ZQ	PAO1 reference with *xcp* operon deletion	Lab. collection
Plasmids		
pCDFDuet-1	Sm^R, 2 MCS, P_{T7}, Ori CDF	Novagen
pETDuet-1	Ap^R, 2 MCS, P_{T7}, Ori f1	Novagen
pET22b	Ap^R, P_{T7}, Ori f1, *pelB* cloning sequence	Novagen
pSp-XcpY$_{Lp}$	pCDFDuet carrying *sp-xcpY$_L$p* gene in MCS 2	This study
pSp-XcpZ$_{Mp}$	pCDFDuet carrying *sp-xcpZ$_M$p* gene in MCS 2	This study
pSp-XcpY$_{Lp}$-Sp-XcpZ$_{Mp}$	pCDFDuet carrying *sp-xcpY$_L$p* in MCS 2 and *sp-xcpZ$_M$p* in MCS1	This study
pCbpD$_H$	pETDuet carrying *cbpD$_H$* gene	This study
pLapA$_H$	pETDuet carrying *lapA$_H$* gene	Lab. collection
pLIC07	pET-28a+ derivative vector for Trx translational fusions Km^R	Bio-Xtal
pLIC-XcpY$_{Lp}$	pLIC07 carrying *xcpY$_L$p*	This study
pLIC-XcpZ$_{Mp}$	pLIC07 carrying *xcpZ$_M$p*	This study
pT7.5-CbpD$_H$	pT7.5 carrying *cbpD$_H$* gene	(47)
pJN105	Gm^R, P_{BAD}, Ori pBR	(48)
pJN105-CbpD	pJN105 carrying *cbpD*	This study
pKT25	Km^R, P_{Lac}, Ori 15A, MCS in the 3' end of T25	(40)
pKNT25	Km^R, P_{Lac}, Ori 15A, MCS in the 5' start of T25	(40)
pUT18C	Ap^R, P_{Lac}, Ori ColE1, MCS in the 3' end of T18	(40)
pUT18	Ap^R, P_{Lac}, Ori ColE1, MCS in the 5' start of T18	(40)
pUT18C-XcpY$_L$	pUT18C carrying *18-xcpY$_L$*	This study
pUT18C-XcpZ$_M$	pUT18C carrying *18-xcpZ$_M$*	This study
pKT25-XcpZfl	pKT25 carrying *25-xcpZ$_M$*	This study
pKT25-XcpSfl	pKT25 carrying *25-xcpS$_F$*	This study
pKT25-Tol	pKT25 carrying *25-tolB* gene	E. Bouveret
pUT18C-Pal	pUT18C carrying *18-pal* gene	E. Bouveret

Table 2 - Oligonucleotides used in this study

Oligo	Sequence 5' → 3'	Characteristics
OSM-86	AGGAGATATACCATGAAATACCTGCTGCCG	*sp-lasB* for MCS1 up
OSM-87	GCCGGGCGGGCCATCGCCGGCTGGGC	*sp-lasB* for MCS1 down
OSM-88	CGATGGCCCGCCCGGCCGAGCGCCAT	*xcpZ$_M$p* for MCS1 up
OSM-91	CCGCAAGCTTGTCGACTCACTCGACCCGCAGGC	*xcpZ$_M$p* for MCS1 down
OSM-62	AAGGAGATATACATATGAAATACCTGCTGCC	*sp-lasB* for MCS2 up
OSM-63	CAGGCCTGGGCCATCGCCGGCTGGGC	*sp-lasB* for MCS2 down
OSM-64	CGATGGCCCAGGCCTGGCAGTTGCAG	*xcpY$_L$p* for MCS2 up
OSM-47	GCGTGGCCGGCCGATATCTCAACCTCCTATCACCAGGC	*xcpY$_L$p* for MCS2 down
OSM-116	CCAATCAATGGAGACCCAGGCCTGGCAGTTGCAG	*xcpY$_L$p* for pLIC07
OSM-117	GTATCCACCTTTACTGGAGACCTCAACCTCCTATCACC	*xcpY$_L$p* for pLIC07
OSM-118	CCAATCAATGGAGACCCGCCCGGCCGAGCGC	*xcpZ$_M$p* for pLIC07
OSM-119	GTATCCACCTTTACTGGAGACCTCACTCGACCCGCAGGCTC	*xcpZ$_M$p* for pLIC07
XcpY$_L$-pUT18C-F	CCCGGATCCCATGAGTGGAGTGAGTGCGCTGTTCC	*xcpY$_L$* for pUT18C
XcpY$_L$-pUT18C-R	GGAATTCTTAGTCAACCTCCTATCACCAGGCGCG	*xcpY$_L$* for pUT18C
XcpZ$_M$-pUT18C-F	CCCGGATCCCATGAAGGTGATGACGCAATTCCACG	*xcpZ$_M$* for pUT18C
XcpZ$_M$-pUT18C-R	GGAATTCTTAGTCACTCGACCCGCAGGCTCAGG	*xcpZ$_M$* for pUT18C
XcpZ$_M$-pKT25-F	CCCGGATCCCATGAAGGTGATGACGCAATTCCACG	*xcpZ$_M$* for pKT25C
XcpZ$_M$-pKT25-R	GGAATTCTTAGTCACTCGACCCGCAGGCTCAGG	*xcpZ$_M$* for pKT25C
XcpS$_F$-pKT25-F	CCCGGATCCCATGGCCGCCTTCGAATACCTCG	*xcpS$_F$* for pKT25C
XcpS$_F$-pKT25-R	GGAATTCTTAGTTACCCCACGAGTTGGTTGAGAG	*xcpS$_F$* for pKT25C

FIGURES LEGENDS

Figure 1. Specific XcpY$_L$/T2SS effector direct interaction. A. Characterization of XcpY$_L$p/CbpD binding using Bio-Layer Interferometry (BLI). Samples of purified XcpY$_L$p and CbpD$_H$ used in BLI experiments were analyzed by 15% SDS-PAGE followed by Coomassie blue staining (up). The graph reporting the BLI response (nm) as function of XcpYp concentration (10-160μM) from three independent experiments was used to calculate the indicated apparent dissociation constant (K$_D$). Each data point (mean +/- SD) is the result from triplicate experiments. **B-C.** Co-purification and immunoblotting experiments of co-produced XcpY$_L$p with his-tagged CbpD (CbpD$_H$) (**B**) or his-tagged LapA (lapA$_H$) (**C**). L: loading material, FT: Flow through, E1 to E5: Elution fractions. Antibodies used for XcpY$_L$, CbpD and LapA detection are indicated in italic below each immunoblotting.

Figure 2. Specific XcpZ$_M$/T2SS effector direct interaction. A. Characterization of XcpZ$_M$p/CbpD binding using Bio-Layer Interferometry (BLI). Samples of previously purified CbpD$_H$ used in experiment presented figure 1 and newly purified XcpZ$_M$p were analyzed by 15% SDS-PAGE followed by Coomassie blue staining and used in BLI experiments. The graph reporting the BLI response (nm) as function of XcpZp concentration (6.25-100μM) from three independent experiments was used to calculate the indicated apparent dissociation constant (K$_D$). Each data point (mean +/- SD) is the result from triplicate experiments. **B-C.** Co-purification and immunoblotting experiments of co-produced XcpZ$_M$p with his-tagged CbpD (CbpD$_H$) (**B**) or his-tagged LapA (lapA$_H$) (**C**). L: loading material, FT: Flow through, E1 to E5: Elution fractions. Antibodies used for XcpZ$_M$, CbpD and LapA detection are indicated in italic below each immunoblotting.

Figure 3. XcpZ$_M$p/XcpY$_L$p binding competition on CbpD. Quantification of CbpD-bounded XcpY$_L$p or XcpZ$_M$p in the eluted fractions (E) compared to their amount in the loaded material (L) in presence, or not, of the second partner XcpY$_L$p or XcpZ$_M$p. The immune-detected bands of XcpY$_L$p and XcpZ$_M$p for each Loaded (L) and eluted (E) fractions of each replicate of the three co-purification experiments are also presented. Molecular weight markers of 10 kDa (▪) and 17 kDa (□) are indicated on the right. (ns) for non-significant, * for Pvalue <0.05.

Figure 4. Effect of CbpD on the AP interactome measured by BACTH. Different combinations of T18/T25 reporter domains fused to the N-domains of full-length Xcp AP components were evaluated by BACTH in presence or not of the Xcp secreted effector CbpD. As a positive control (T(+)), we used the couple T18-Tol/T25-Pal (46). The value of the negative control (T(-)) corresponds to the mean of all T18/T25 combinations containing Xcp constructs against the T18-Tol/T25-Pal. Results are expressed in Miller units of β-galactosidase activity and are the mean ± standard deviation of at least three independent experiments. The red line indicates the background β-galactosidase activity measured in the negative control. (ns) for non-significant, * for Pvalue <0.05 and ** for Pvalue <0.01.

Figure 5. Schematic representation of the effector-sensing step mediated by XcpY$_L$/Z$_M$ during secretion process by T2SS. ❶ Effector binding to the periplasmic domains of GspL$_Y$ (L) and GspM$_Z$ (M) induces their homo- and/or hetero-oligomerization (purple arrows). ❷ The effector-mediated gathering of GspM$_Z$ and GspL$_L$ generates a transmembrane signal (red flash) triggering GspE$_R$ (E) activation (ATP to ADP) and pseudopilus (GspG$_T$H$_U$I$_V$J$_W$K$_X$ (GHIJK)) assembly and elongation (dashed red arrows). ❸ The growing pseudopilus interacts with the effector, which first transfers it inside the vestibule of the secretin, and then leads to its translocation in the extracellular milieu. Also represented on this cartoon are the

15

secretin connector GspC$_P$ (C) and the politopic AP component GspF$_S$ (F), which is involved in pseudopilus assembly upon cycles of GspE$_R$-mediated rotation (circular red arrows).
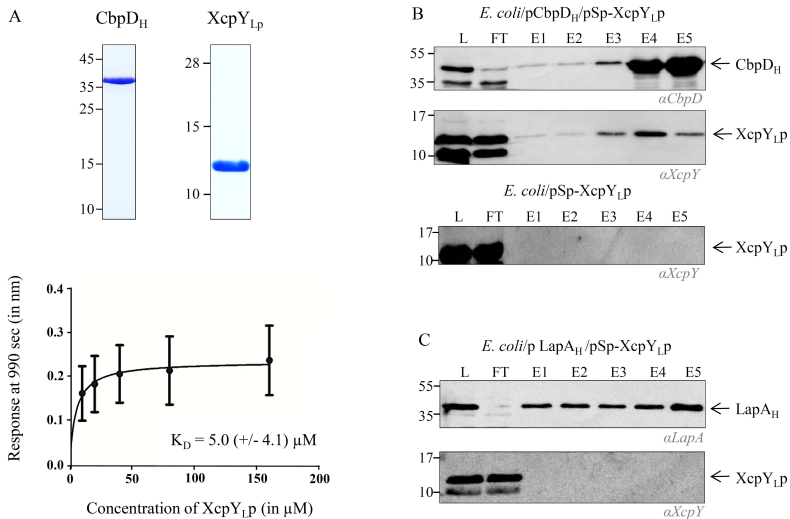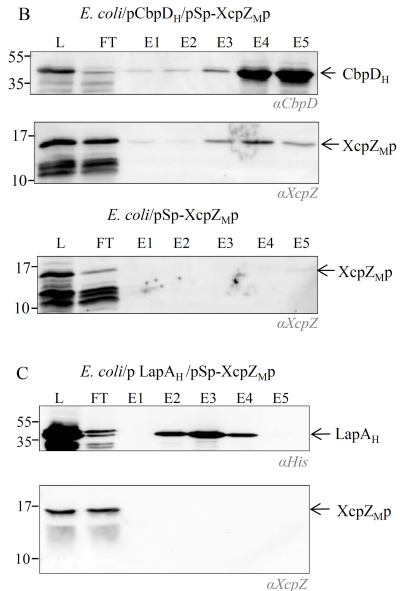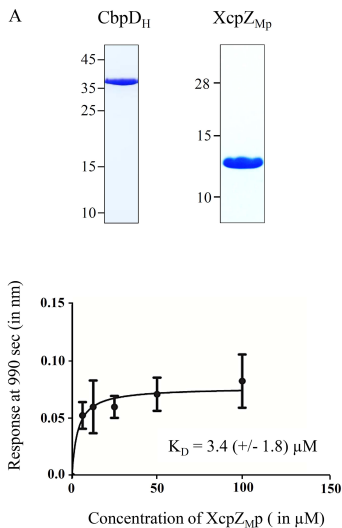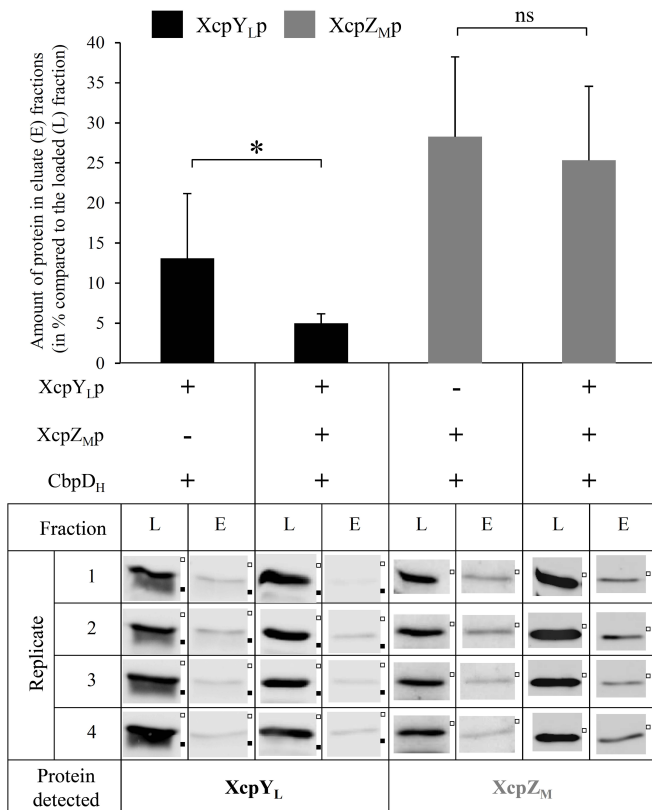
Figure 1

Figure 2

A

CbpD$_H$ XcpZ$_{Mp}$

K$_D$ = 3.4 (+/- 1.8) µM

B *E. coli*/pCbpD$_H$/pSp-XcpZ$_{Mp}$

← CbpD$_H$
αCbpD

← XcpZ$_{Mp}$
αXcpZ

E. coli/pSp-XcpZ$_{Mp}$

← XcpZ$_{Mp}$
αXcpZ

C *E. coli*/p LapA$_H$ /pSp-XcpZ$_{Mp}$
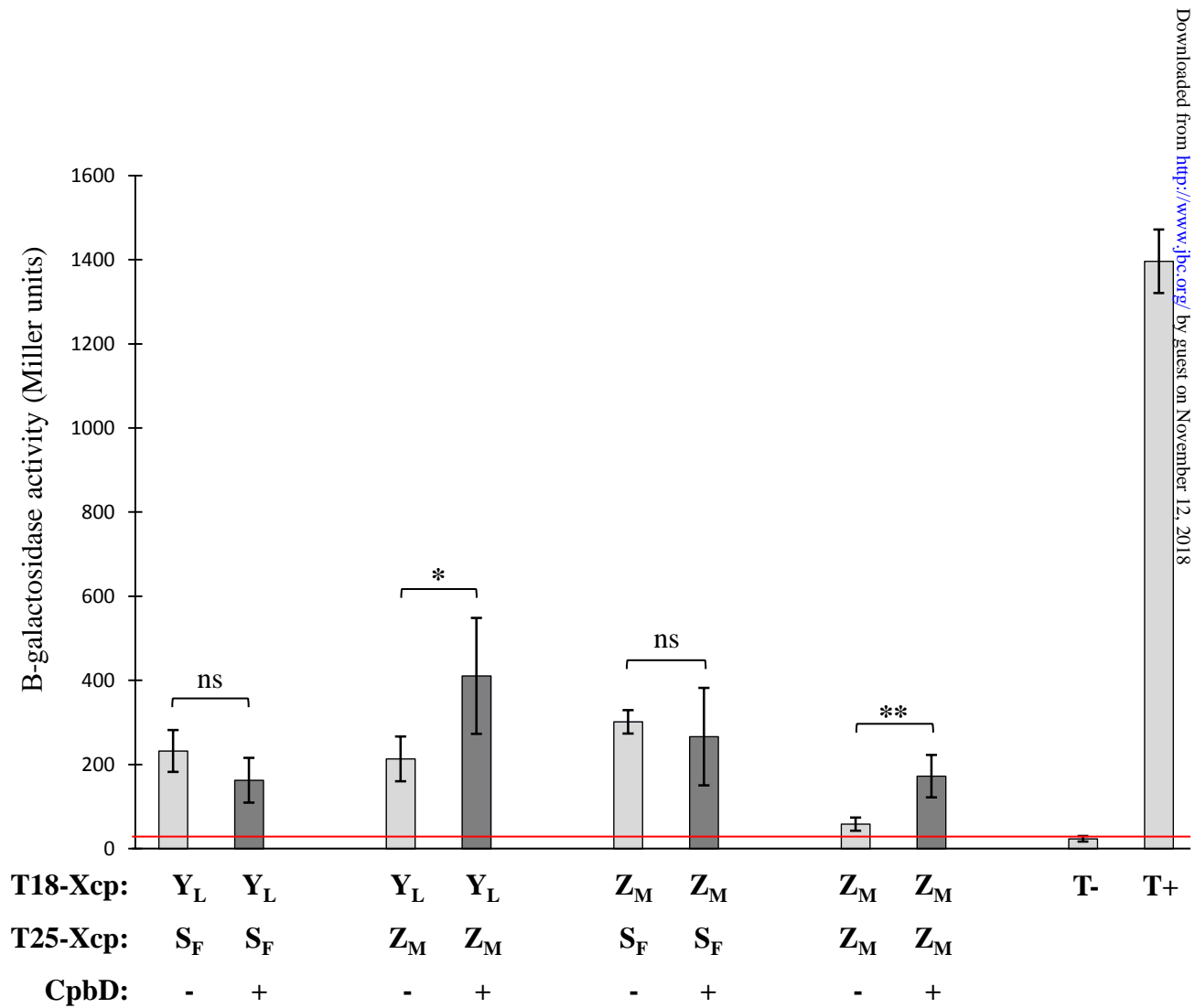
← LapA$_H$
αHis
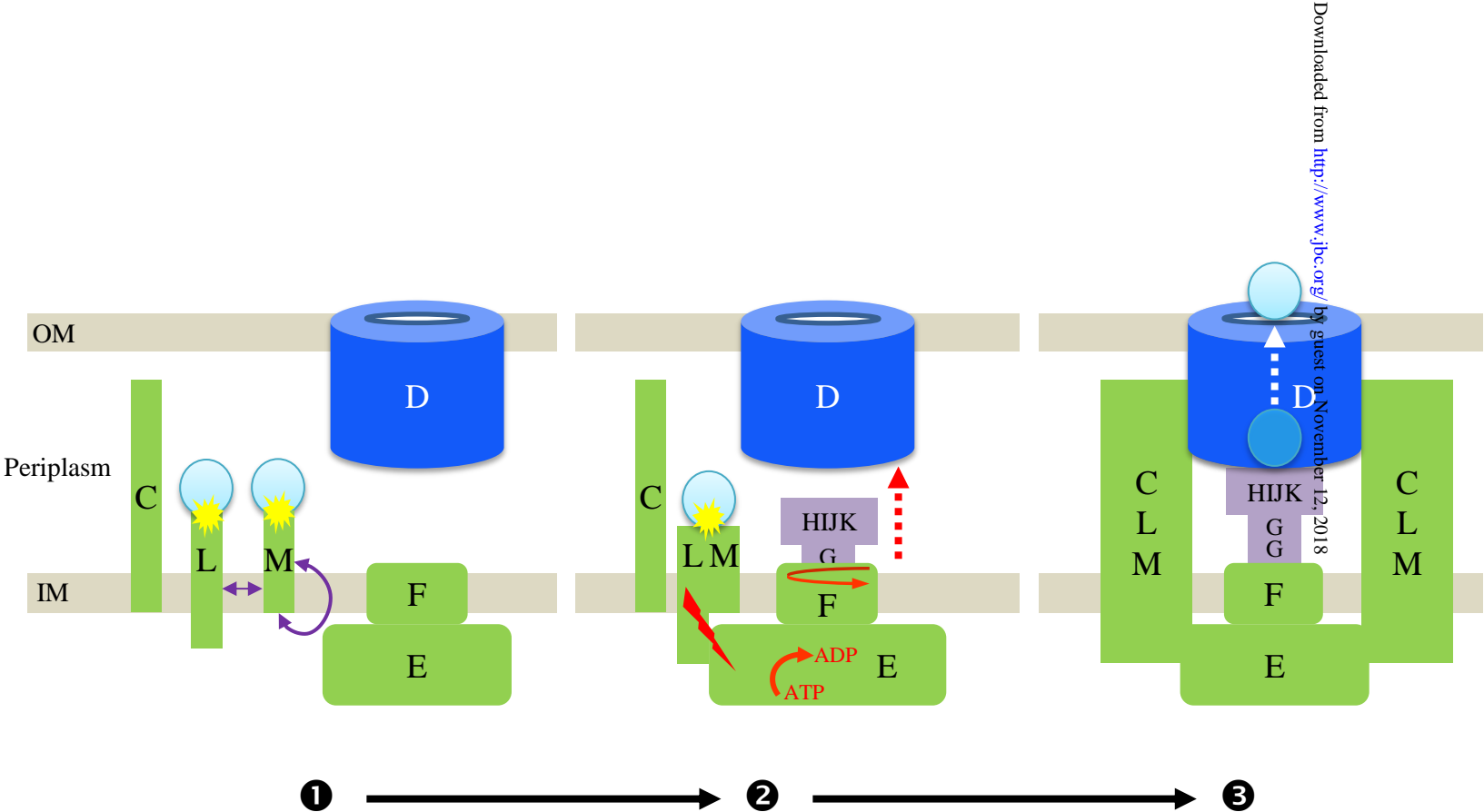
← XcpZ$_{Mp}$
αXcpZ

Figure 3

Figure 4

Figure 5

Direct interactions between the secreted effector and the T2SS components GspL and GspM reveal a new effector-sensing step during type 2 secretion

Sandra Michel-Souzy, Badreddine Douzi, Frédéric Cadoret, Claire Raynaud, Loïc Quinton, Geneviève Ball and Romé Voulhoux

J. Biol. Chem. published online October 18, 2018

Access the most updated version of this article at doi: 10.1074/jbc.RA117.001127

Alerts:
- When this article is cited
- When a correction for this article is posted

Click here to choose from all of JBC's e-mail alerts